nature biomedical engineering

ARTICLES

https://doi.org/10.1038/s41551-021-00767-0

Check for updates

A soft neuroprosthetic hand providing simultaneous myoelectric control and tactile feedback

Guoying Gu[1,2,5]✉, Ningbin Zhang[1,5], Haipeng Xu[1], Shaoting Lin[3], Yang Yu[1], Guohong Chai[1], Lisen Ge[1], Houle Yang[1], Qiwen Shao[1], Xinjun Sheng[1,2], Xiangyang Zhu[1,2,5]✉ and Xuanhe Zhao[3,4,5]✉

Neuroprosthetic hands are typically heavy (over 400 g) and expensive (more than US$10,000), and lack the compliance and tactile feedback of human hands. Here, we report the design, fabrication and performance of a soft, low-cost and lightweight (292 g) neuroprosthetic hand that provides simultaneous myoelectric control and tactile feedback. The neuroprosthesis has six active degrees of freedom under pneumatic actuation, can be controlled through the input from four electromyography sensors that measure surface signals from residual forearm muscles, and integrates five elastomeric capacitive sensors on the fingertips to measure touch pressure so as to enable tactile feedback by eliciting electrical stimulation on the skin of the residual limb. In a set of standardized tests performed by two individuals with transradial amputations, we show that the soft neuroprosthetic hand outperforms a conventional rigid neuroprosthetic hand in speed and dexterity. We also show that one individual with a transradial amputation wearing the soft neuroprosthetic hand can regain primitive touch sensation and real-time closed-loop control.

There are more than 5 million individuals with upper-limb amputations worldwide. Losing a hand is generally catastrophic, seriously limiting a person's ability in daily activities[1–6]. Although artificial prostheses are available, the most widely used prostheses are still cosmetic devices or functional hook-like grippers. Although a few anthropomorphic neuroprosthetic hands[1,2,7] (such as the i-Limb Hand, the Michelangelo Hand, the Bebionic Hand and the Vincent Hand) have been commercialized, they all rely on electrical motors and sophisticated mechanical components. The high weights (>400 g) and high cost (>US$10,000) of these neuroprosthetic hands severely limit their broad use for individuals with amputations[3,4]. It is also desirable for neuroprosthetic hands to have the compliance and tactile feedback of human hands[1,2,5]. For example, the Pisa/IIT SoftHand[8–10], which is composed of electrical motors and tendon-driven mechanisms with compliant joints and soft skins, has been developed as a myoelectric prosthesis with high compliance and a high weight of 520 g. Several recent studies[11–18] have investigated the invasive or non-invasive sensory feedback for individuals with upper-limb amputations, but the sensory feedback is implemented only in rigid neuroprosthetic hands. The emerging field of soft robotics[19–21] that combines the compliance of human skins and muscles with the simple design and fabrication of lightweight elastomeric components may open a promising avenue for future neuroprosthetic hands. Many bioinspired soft robotic systems such as locomotive robots[22], finger-like actuators[23–26], robotic exoskeletons[27–29] and hands[30–34] have been developed (Supplementary Table 1).

In this Article, we report the design, fabrication and performance of a lightweight (292 g) and potentially low-cost (cost of components of less than US$500) soft neuroprosthetic hand that is capable of simultaneous myoelectric control and tactile feedback for use by individuals with transradial amputations (Fig. 1a and Supplementary Tables 2 and 3). The soft neuroprosthetic hand consists of five soft fingers and a palm that provide six active degrees of freedom (d.f.), four electromyography sensors that measure the surface electromyogram (EMG) signals of residual forearm muscles to control the hand to deliver four common grasp types, and five hydrogel–elastomer capacitive sensors on the fingertips that measure touch pressure so as to elicit electrical stimulation on the skin of the residual limb. To evaluate the functions of the soft neuroprosthetic hand, two individuals with transradial amputations performed a set of standardized tests[6] (including the Box and Blocks Test, all seven tasks in the Jebsen–Taylor Hand Function Test and nine selected tasks in the Southampton Hand Assessment Procedure). One individual with a transradial amputation wearing the soft neuroprosthetic hand demonstrated the dexterous and versatile functions of the hand, with primitive tactile sensation and closed-loop control in daily activities such as handling tools, eating, shaking hands, petting animals and recognizing touch pressure.

Design

Hand. Each finger of the soft neuroprosthetic hand is based on a fibre-reinforced elastomeric tubular structure, in which two or three rigid segments with specific lengths are embedded to mimic the soft-joint/rigid-bone anatomy of the thumb or other fingers, respectively, of a human hand[35,36] (Fig. 1b and Supplementary Figs. 1 and 2). The thumb–palm connection in the soft neuroprosthetic hand is based on a fibre-reinforced elastomeric hollow pad with a strain-limiting layer (Supplementary Fig. 3). The soft neuroprosthetic hand is designed to possess six active d.f. (Fig. 1c): each soft finger can be pneumatically actuated to provide one flexion d.f. and the thumb–palm connection under pneumatic actuation further gives the thumb another circumduction d.f. Furthermore, the inherent compliance of the soft fingers can introduce many passive d.f. to the soft hand for dexterous and adaptive grasps even on

[1]Robotics Institute, School of Mechanical Engineering, Shanghai Jiao Tong University, Shanghai, China. [2]State Key Laboratory of Mechanical System and Vibration, Shanghai Jiao Tong University, Shanghai, China. [3]Department of Mechanical Engineering, Massachusetts Institute of Technology, Cambridge, MA, USA. [4]Department of Civil and Environmental Engineering, Massachusetts Institute of Technology, Cambridge, MA, USA. [5]These authors contributed equally: Guoying Gu, Ningbin Zhang, Xiangyang Zhu, Xuanhe Zhao. ✉e-mail: guguoying@sjtu.edu.cn; mexyzhu@sjtu.edu.cn; zhaox@mit.edu

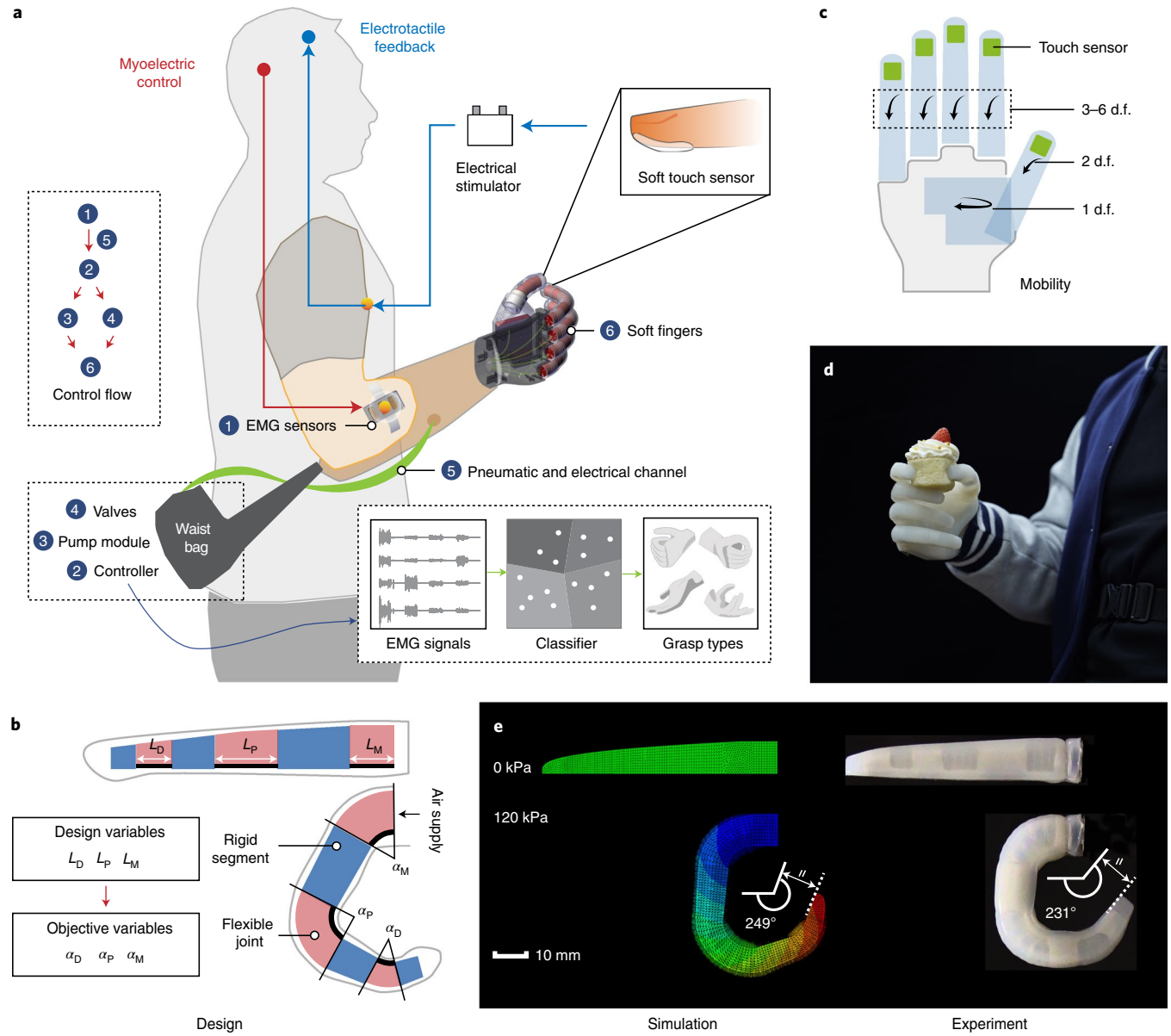

Fig. 1 | Design and operation of the soft neuroprosthetic hand. a, Illustration of the soft neuroprosthetic hand worn by an individual with a transradial amputation with a waist bag. The soft neuroprosthetic hand consists of five soft fingers and a palm, four electromyography sensors that measure the surface EMG signals of residual forearm muscles to control the hand, and five hydrogel–elastomer capacitive sensors on the fingertips that measure touch pressure to elicit electrical stimulation on the skin of the residual limb. By integrating the EMG sensors, touch sensors and electrical stimulators in the hand, we developed a bidirectional human–machine interface for the soft neuroprosthetic hand. **b**, The working principle of a soft finger made of a fibre-reinforced elastomeric tubular structure, in which three rigid segments with specific lengths are embedded to mimic the soft-joint/rigid-bone anatomy of the human finger. Our design objective is to generate the desired bending angles (α_D, α_P, α_M) of the flexible joints by tuning their lengths (L_D, L_P, L_M). The subscripts D, P and M indicate distal interphalangeal, proximal interphalangeal and metacarpophalangeal, respectively. **c**, Schematic of the soft neuroprosthetic hand with six active d.f. motions and five soft capacitive touch sensors on the fingertips. **d**, Photograph of an individual with a transradial amputation wearing the soft neuroprosthetic hand grabbing a cupcake. **e**, Simulation of the finite-element model (left) and experimental result of a soft finger (right) under an applied pneumatic pressure of 120 kPa. The '//' symbols indicate that the solid line and the dashed line are parallel. Scale bar, 10 mm.

fragile and soft objects (Fig. 1d), mimicking the passive compliance of human hands[8].

We chose the pneumatically actuated soft fingers owing to their advantages of low cost, light weight and scalable fabrication[21]. As the applied pneumatic pressure to a soft finger increases, the bending angles of the flexible joints increase. We developed an analytical model to study the bending angles of a soft finger's flexible joints (see the 'Analytical model for the design of the soft finger' section in the Methods). The model demonstrates that, with a fixed finger length, the bending angles of the flexible joints are linearly proportional to the lengths of the flexible joints. This trend is consistent with the experimental results (Supplementary Figs. 4 and 5). We further developed a finite-element model to quantitatively predict the bending angles of the flexible joints and the deformation of the soft finger after pneumatic actuation (see the 'Finite-element model for the design of the soft finger' section in the Methods).

The finite-element model is in quantitative agreement with the experimental results (Fig. 1e, Supplementary Fig. 6 and Supplementary Video 1). For example, the finite-element model predicted that the three flexible joints in the soft index finger under the maximum pneumatic actuation of 120 kPa give the bending angles of 84.02°, 112.58° and 52.55°, deviating from the experimental results by only 3.25%, 11.60% and 7.44%, respectively (Supplementary Table 4).

The five soft fingers are mounted onto a three-dimensionally (3D) printed plastic palm (Imagine 8000) in the shape of a human palm. Both the fingers and the palm are covered by a soft elastomeric layer mimicking the skin on the human hand. The palm skeleton is further connected to a customized plastic socket that fits with the residual limb of the individual with a transradial amputation. Owing to the pneumatic actuation and modular design of the soft neuroprosthetic hand, the pumps, valves, electronic boards and battery for the hand can be contained in a small bag (total weight of 444 g) on the waist of the individual with an amputation (Supplementary Fig. 7a). The pumps and electronic board are connected by soft tubing and electrical wires (hidden under clothes and in the socket) to the soft fingers and sensors on the hand, respectively. This modular design can substantially reduce the weight of the soft neuroprosthetic hand to 292 g, which is much lighter than the weights of commercially available neuroprosthetic hands (420–628 g; Supplementary Table 3) and the average human hands (400 g)[1,2]. Notably, as the commercially available neuroprosthetic hands integrate the electric motors, transmission mechanisms and batteries in their palms and sockets, it is challenging to significantly reduce their weights. We further demonstrate that the six active d.f. of the soft neuroprosthetic hand can be independently controlled with one pump and twelve valves (Supplementary Video 2). If needed, we can also integrate the pumps, valves, electronic boards and battery into the socket of the soft neuroprosthetic hand (Supplementary Fig. 7b); such a design increases the weight of the soft neuroprosthetic hand to 604 g, which is still lighter than or comparable to the weights of commercially available neuroprosthetic hands such as the i-Limb large hand and the Bebionic medium hand (Supplementary Table 3).

EMG sensors. In the socket of the hand, we implement four customized EMG sensors (Fig. 1a and Supplementary Fig. 8), which will be mounted onto the skin of the residual limb to record the surface EMG signals from the target muscles in the residual limb. Each EMG sensor (weight of 10 g) consists of three electrodes (a reference electrode and a pair of differential electrodes) and the readout electronics (including the two-level signal amplifier and filter circuits; Supplementary Fig. 9). The locations of the EMG sensors with respect to the target muscles have been optimized to achieve a superior performance on decoding the motion intention of the individual with an amputation. The decoded motion intention will be used to control the soft fingers and palm to deliver the corresponding grasp types.

Touch sensors and electrical stimulators. To sense the touch pressure of the soft neuroprosthetic hand applying on objects, we implemented five soft capacitive touch sensors, each on a fingertip of the hand (Fig. 1c). The capacitive touch sensor is composed of an ionic hydrogel–elastomer hybrid structure[37–39] that forms a capacitor for sensing the touch pressure (Supplementary Fig. 10a). An increase in the touch pressure reduces the thickness of the elastomeric layer and therefore increases the capacitance of the capacitor (Supplementary Fig. 10b). The measured relative capacitance change is used to control an electrical stimulator (Supplementary Fig. 11), which outputs programmable electrical pulses through a non-invasive stimulation electrode on a specific region of the residual limb (Supplementary Fig. 12) to inform the individual with an amputation of the touch pressure on the corresponding fingertip.

Control algorithm. By integrating the EMG sensors, touch sensors and electrical stimulators in the hand, we developed a bidirectional human–machine interface for the soft neuroprosthetic hand (a description of the experimental set-up is provided in Supplementary Fig. 11). We chose a pattern-recognition approach[40] to classify the surface EMG signals into five classes corresponding to the four common grasp types[41,42] and rest type of human hands (descriptions of the pattern recognition algorithms are provided in the Supplementary Information). The decoded grasp types are then mapped onto the actuation command for the corresponding soft fingers and palm. On the basis of the relative changes in the measured capacitances of the capacitive touch sensors (caused by the touch pressure), we can program the electrical stimulator to output the corresponding stimulation patterns, which inform the individual with an amputation of the touch pressure on each fingertip. On the basis of the informed touch pressure, the individual can further change the grasp type of the soft neuroprosthetic hand by varying the EMG signals, therefore forming a closed-loop control of the hand.

Characterization

We used a simple and scalable method to fabricate and assemble the soft neuroprosthetic hand (see the 'Fabrication and assembly of the soft neuroprosthetic hand' section in the Methods; Supplementary Fig. 13). We next characterized the performance of the fabricated soft neuroprosthetic hand. To monitor its kinematics, we developed a motion-tracking system (Supplementary Fig. 14). For the 1 d.f. flexion fingers (that is, index, middle, ring and little fingers), we attached markers to their flexible joints and fingertips to measure the bending angles of the joints and the fingertips (Fig. 2a). We found that an increase in the applied pneumatic pressure increased the bending angle of the fingertip to a maximum of 231° at 120 kPa pneumatic pressure (Fig. 2b). Furthermore, the measured bending angles of the flexible joints are consistent with the prediction of the finite-element model (Fig. 2b, Supplementary Fig. 6a and Supplementary Table 4). For the 2 d.f. thumb, we attached markers to its flexible joints, thumb tip and thumb–palm connection (Fig. 2c). The results indicate that the thumb has a maximum flexion of 69° and a maximum palm circumduction of 28° at 80 kPa pneumatic pressure, which also agrees well with the finite-element model's prediction (Fig. 2d, Supplementary Figs. 6b and 15, and Supplementary Table 4). The maximum bending angles of the soft fingers are comparable to those of existing rigid counterparts (Supplementary Table 3).

To evaluate the load capacity of the soft neuroprosthetic hand, we used the hand (at 100 kPa pneumatic pressure to the 1 d.f. fingers and 80 kPa pneumatic pressure to the 2 d.f. thumb) to grasp a cylinder (diameter, 55 mm) while measuring the grasping force with an electronic dynamometer (Supplementary Fig. 16). The results indicate that the soft neuroprosthetic hand gives maximum grasping forces of 18 N and 17 N along the vertical and horizontal directions, respectively (Fig. 2e,f). Thus, the soft neuroprosthetic hand can perform most grasping tasks in daily activities, which generally require grasping forces of less than 10 N for human hands[43]. The grasping forces of the soft fingers can potentially be increased in future studies by using stiffer elastomers for the fingers and applying higher pneumatic pressures.

Furthermore, we demonstrate that our soft fingers have repeatable pressure–flexion relationships with small hysteresis over 10,000 cycles of actuations (Fig. 2g). The soft fingers are also resilient when being bent to arbitrary angles, struck with a steel hammer and run over back and forth by one wheel of a 1,500 kg vehicle (Supplementary Fig. 17 and Supplementary Video 3).

On the basis of the usage frequencies of the grasp types in daily activities[41,42], we chose to recognize the most commonly used four

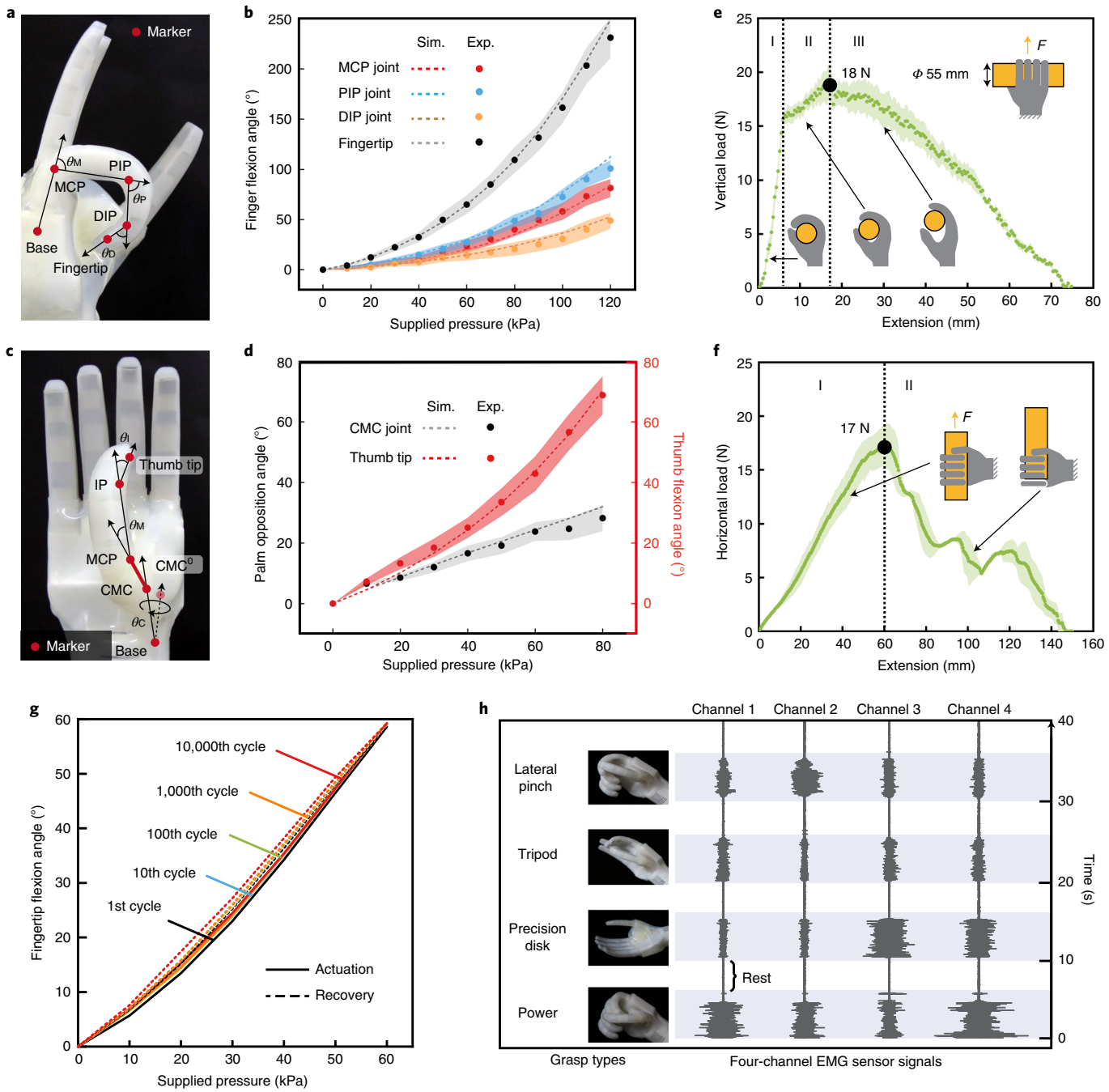

Fig. 2 | Performance characterization of the soft neuroprosthetic hand. a–d, Measurement schematics (**a**,**c**) and results (**b**,**d**) of the ranges of motions for the 1 d.f. flexion fingers (**a**,**b**), and for the 2 d.f. opposable thumb (**c**,**d**). Data are mean ± s.d. of $n = 3$ measurements at each data point. The dashed lines represent the predictions of the finite-element model. In **a** and **c**, CMC^0 indicates the initial position of the CMC joint, θ_I indicates the IP joint angle; θ_M indicates the MCP joint angle, θ_C represents the CMC joint angle, θ_D indicates the DIP joint angle and θ_P indicates the PIP joint angle. CMC, carpometacarpal; DIP, distal interphalangeal; Exp., experiment; IP, interphalangeal; MCP, metacarpophalangeal; PIP, proximal interphalangeal; Sim., simulation. **e**,**f**, Vertical (**e**) and horizontal (**f**) load capability tests of the soft neuroprosthetic hand by grasping a 55-mm-diameter cylinder at 100 kPa pneumatic pressure to the 1 d.f. flexion fingers and 80 kPa pneumatic pressure to the 2 d.f. thumb. During these tests, the soft neuroprosthetic hand was fixed to the air bearing testbed and the horizontal handle and vertical handle are positioned at the rigid palm. Then, the soft fingers are actuated to the predefined pressures and the linear stage pulls the handle at a fixed velocity (1 mm s^{-1}) until the handle separates from the hand. **g**, Pressure–flexion hysteresis curves for the soft finger in the 1st, 10th, 100th, 1,000th and 10,000th cycles of actuations with the actuation frequency of 0.2 Hz. **h**, The four-channel EMG signals from the residual forearm muscles to decode the grasp intention (for example, the four grasp types of power, precision disk, tripod and lateral pinch, and rest). In **a** and **e**, θ indicates the joint angle and Φ indicates the diameter of the cylinder.

grasp types (that is, power, precision disk, tripod and lateral pinch) of individuals with amputations through the myoelectric control interface (Supplementary Fig. 18). Using the four-channel EMG sensors (one sensor at each channel), the soft neuroprosthetic hand can decode the intended four grasp types and rest type (Fig. 2h and Supplementary Fig. 19).

We next calibrated the capacitive touch sensor by uniformly compressing the sensor and then measuring its capacitance. Under

zero pressure, we denote the measured capacitance of the sensor as C_0. With the increase in the applied pressure, we can obtain the current capacitance C of the touch sensor and calculate the change of the capacitance $\Delta C = C - C_0$. The experimental results demonstrate that, when the uniformly applied pressure on the sensor increases from 0 kPa to 55.8 kPa, the $\Delta C/C_0$ varies from 0 to 0.85, giving a sensitivity of 0.016 kPa^{-1} (Supplementary Fig. 10b).

Performance on individuals with amputations

Performances with soft and rigid neuroprosthetic hands. The soft neuroprosthetic hand can restore the versatile hand functions for individuals with amputations. An individual with a transradial amputation can adapt to the soft neuroprosthetic hand and master its functions after training for 15 min (Supplementary Fig. 20 and Supplementary Video 4). We used a set of standardized tests[6] to evaluate the performances of the soft neuroprosthetic hand (Fig. 3a, Supplementary Fig. 21 and Supplementary Video 5), including the Box and Blocks Test (that is, counting the number of blocks that can be grasped and transported per minute), all seven tasks in the Jebsen–Taylor Hand Function Test (that is, J1, writing; J2, simulated page-turning; J3, lifting small common objects; J4, simulated feeding; J5, stacking checkers; J6, lifting large light objects; and J7, lifting large heavy objects), and nine selected tasks in the Southampton Hand Assessment Procedure (that is, grasping nine kinds of objects, including the following: S1, spherical light; S2, spherical heavy; S3, tripod light; S4, power light; S5, power heavy; S6, tip light; S7, tip heavy; S8, extension light; and S9, extension heavy). As a comparison, the same individual wearing a conventional rigid neuroprosthetic hand[7] trained by the same amount of time (about 15 min) performed the same set of standardized tests (Supplementary Fig. 22 and Supplementary Video 6). Throughout the tests, the individual feels that the soft neuroprosthetic hand is much lighter to wear than the rigid neuroprosthetic hand. Statistical analyses (Fig. 3a and Supplementary Table 5) further demonstrate that, compared with the rigid neuroprosthetic hand, the soft neuroprosthetic hand has significantly superior performances in 7 items (that is, Box and Blocks Test, J3, J4, J7, S1, S3 and S5), significantly inferior performances in 3 items (that is, J5, S6 and S7) and statistically similar performances ($P > 0.05$) in 7 items (that is, J1, J2, J6, S2, S4, S8 and S9). On the basis of the same set of standardized tests and statistical analyses (Supplementary Fig. 23 and Supplementary Table 6), another individual with a transradial amputation demonstrates that the performances of the soft neuroprosthetic hand are significantly superior in 5 items (that is, J3, J5, S4, S5 and S8), significantly inferior in 4 items (that is, J1, S6, S7 and S9) and statistically similar in 8 items (that is, Box and Blocks Test, J2, J4, J6, J7, S1, S2 and S3) compared to those of the rigid counterpart[45–47] (Supplementary Fig. 23).

Next, we performed comparative experiments for the same individual wearing the soft neuroprosthetic hand and the rigid i-Limb hand to grasp fragile objects (for example, strawberry, bread and paper cup). The results indicate that the rigid neuroprosthetic hand damages the strawberry and bread, and tends to crush the paper cup (Supplementary Fig. 24a and Supplementary Video 7). Owing to the inherent compliance, the soft neuroprosthetic hand can guarantee safe interactions with these fragile and soft objects (Supplementary Fig. 24b and Supplementary Video 7).

Furthermore, we demonstrate that one individual wearing the soft neuroprosthetic hand can intuitively perform the four common grasp types to grasp different objects (Supplementary Video 8) and handle commonly used items in daily activities, such as food (for example, crisps, cakes, strawberries and apples), commodities (for example, clothes, bags, laptops, water glasses, bottles, tissues and dishes) and tools (for example, hammers and pliers). The individual also achieves safe interactions with other individuals (for example, shaking hands), animals (for example, petting a cat) and environments (for example, touching a flower) (Fig. 3b and Supplementary Video 9). We further demonstrate that the individual can carry out delicate tasks to handle objects with complex shapes and different sizes and then insert them in the corresponding slots precisely (Fig. 3c and Supplementary Video 10). In a load test, the individual wearing the soft neuroprosthetic hand can lift a payload of 2.3 kg (Fig. 3d and Supplementary Video 11).

Tactile feedback and closed-loop control. Human hands can feel the touch pressure when grasping objects, but most existing prosthetic hands do not possess such tactile feedback[11–18]. Here we demonstrate that the individual wearing the soft neuroprosthetic hand can restore primitive touch sensation based on the capacitive touch sensors and electrical stimulators. When the effective pressure on the touch sensor of a fingertip reaches a threshold (that is, threshold $\Delta C/C_0$), the electrical stimulator will be triggered to generate an electrical pulse (amplitude of 4.0 mA, pulse width of 200 μs and pulse frequency of 20 Hz) to stimulate a specific region on the residual limb corresponding to the fingertip (Fig. 4a and Supplementary Fig. 12). We set the threshold effective pressure at 2.3 kPa (that is, the threshold $\Delta C/C_0 = 0.1$), such that the touch sensors are sufficiently sensitive to touch pressures commonly experienced in daily activities[44], yet are unaffected by environmental noises or crosstalk among sensors (Supplementary Fig. 25). In a blindfolded and acoustically shielded interaction experiment, we gently compressed the five fingers of the soft neuroprosthetic hand in random combinations. The individual can almost instantaneously distinguish any individual finger or multiple fingers being compressed (Fig. 4b and Supplementary Video 12).

Next, we demonstrate the closed-loop control capability of the soft neuroprosthetic hand enabled by integrating the myoelectric control and the tactile feedback. In a blindfolded and acoustically shielded experiment, the individual used his own EMG signals to control the soft neuroprosthetic hand to give the power grasp type. If the hand firmly grasped a bottle such that the effective pressures on the five fingertips were above the threshold, the individual was informed by the electrical stimulators to lift up the bottle (Fig. 4c,d and Supplementary Video 13). By contrast, if the hand did not grasp anything that applied pressure on the fingertips, the individual did not lift, but relaxed the hand after a few seconds (Fig. 4c,d and Supplementary Video 13).

Furthermore, by programming the frequencies (that is, 5 Hz, 20 Hz or 35 Hz) of the electrical pulses to map different ranges of $\Delta C/C_0$ of the touch sensor on the middle finger (that is, no stimulation when $\Delta C/C_0 \leq 0.1$, 5 Hz when $0.1 < \Delta C/C_0 \leq 0.3$, 20 Hz when $0.3 < \Delta C/C_0 \leq 0.4$ and 35 Hz when $\Delta C/C_0 > 0.4$), we demonstrate that, in the blindfolded and acoustically shielded experiment, the individual can restore the graded tactile feedback to discriminate three cylinders with different diameters (that is, 60 mm, 70 mm and 80 mm) with an accuracy of 96.25% (Supplementary Fig. 26 and Supplementary Video 14).

Discussion

We have shown a soft neuroprosthetic hand for individuals with transradial amputations that restores versatile hand functions and primitive tactile sensation. We chose a modular design to enable efficient design iterations, fabrication and control, as well as rapid replacement of the components in case of wear or damage. Compared with commercially available neuroprosthetic hands, the soft neuroprosthetic hand has a number of advantages, including its intrinsic compliance, light weight (292 g), potentially low cost (component cost below US$500) and embedded soft touch sensors. The soft neuroprosthetic hand also maintains a similar number of active d.f. and joints, as well as the maximum bending angles of the joints (Supplementary Table 3) compared to the commercial counterparts. When fitted on individuals with transradial amputations, we used the most commonly used EMG-decoding algorithm as well as electrotactile feedback.

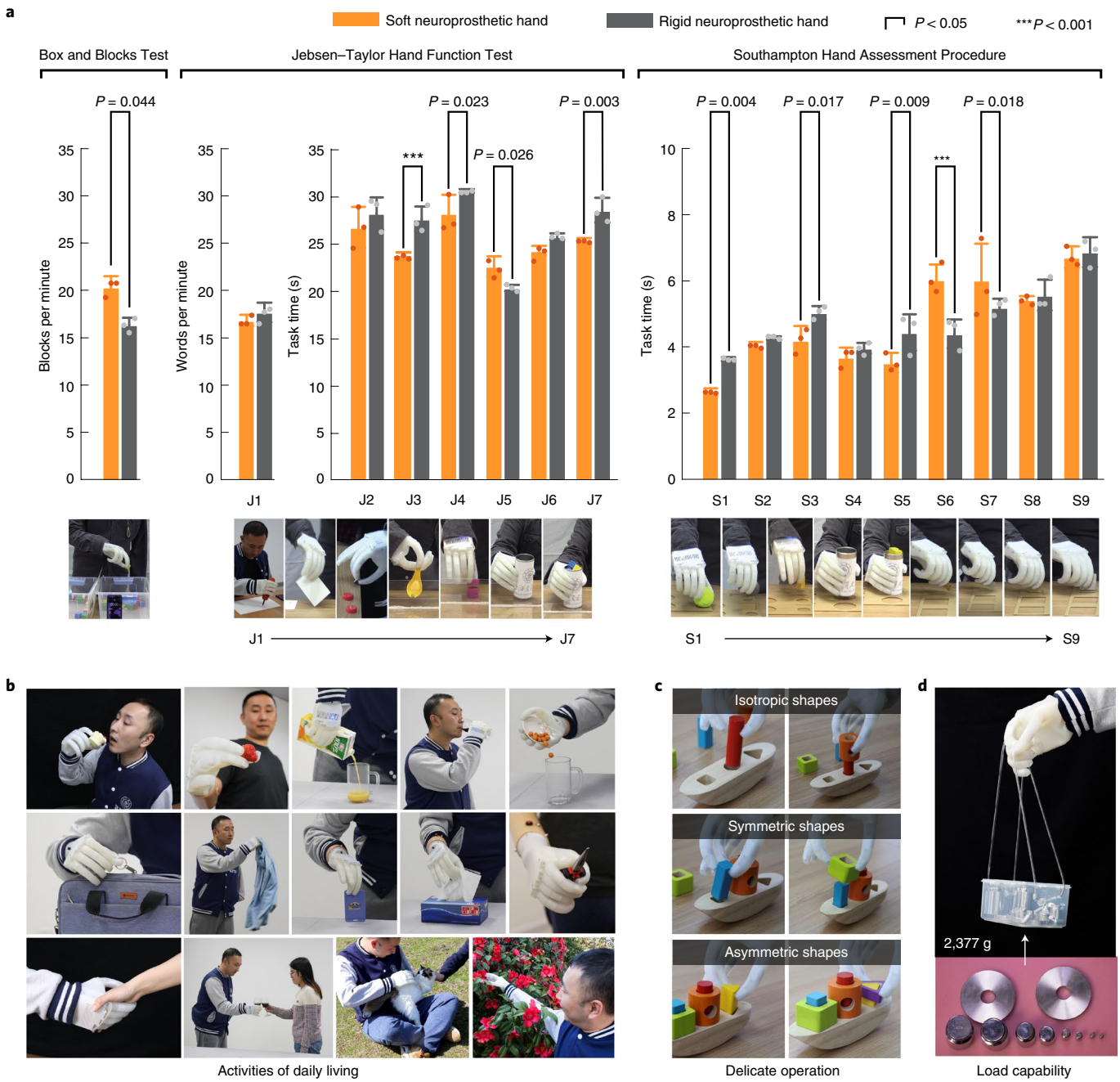

Fig. 3 | An individual with a transradial amputation wearing the soft neuroprosthetic hand, restoring the versatile hand functions in daily activities. **a**, Evaluation of the soft neuroprosthetic hand with a set of standardized tests, including the Box and Blocks Test (for example, counting the number of blocks per minute), all seven tasks in the Jebsen–Taylor Hand Function Test (J1, writing; J2, simulated page-turning; J3, lifting small common objects; J4, simulated feeding; J5, stacking checkers; J6, lifting large light objects; and J7, lifting large heavy objects), and nine selected tasks of the Southampton Hand Assessment Procedure (for example, grasping nine kinds of objects, such as: S1, spherical light; S2, spherical heavy; S3, tripod light; S4, power light; S5, power heavy; S6, tip light; S7, tip heavy; S8, extension light; and S9, extension heavy). Data are mean ± s.d. $n = 3$. $P < 0.05$ was considered to be statistically significant. Note that two-way analysis of variance (ANOVA) was used to statistically analyse the significant influences of the two factors (neuroprosthetic hand types and task types) on the task time in items J2–J7 and S1–S9, respectively. Bonferroni correction was applied to correct for multiple comparisons. Two-tailed, paired-samples *t*-tests were used to compare the difference in blocks per minute (in the Box and Blocks Test) and words per minute (item J1) with different neuroprosthetic hand types, respectively. ***$P < 0.001$. **b**, Photographs of grasping and manipulating commonly used items in daily activities, such as food (for example, cakes and strawberries), commodities (for example, clothes, bags, water glasses and tissues) and tools (for example, pliers), and safe interaction with the environment (for example, shaking a hand, petting a cat and touching a flower). **c**, Photographs of an individual carrying out delicate tasks in which the individual handled objects with complex shapes and different sizes and then inserted them into the corresponding slots precisely. **d**, Photograph of an individual lifting a payload of about 2.3 kg (the presented image is one of three experimental trials).

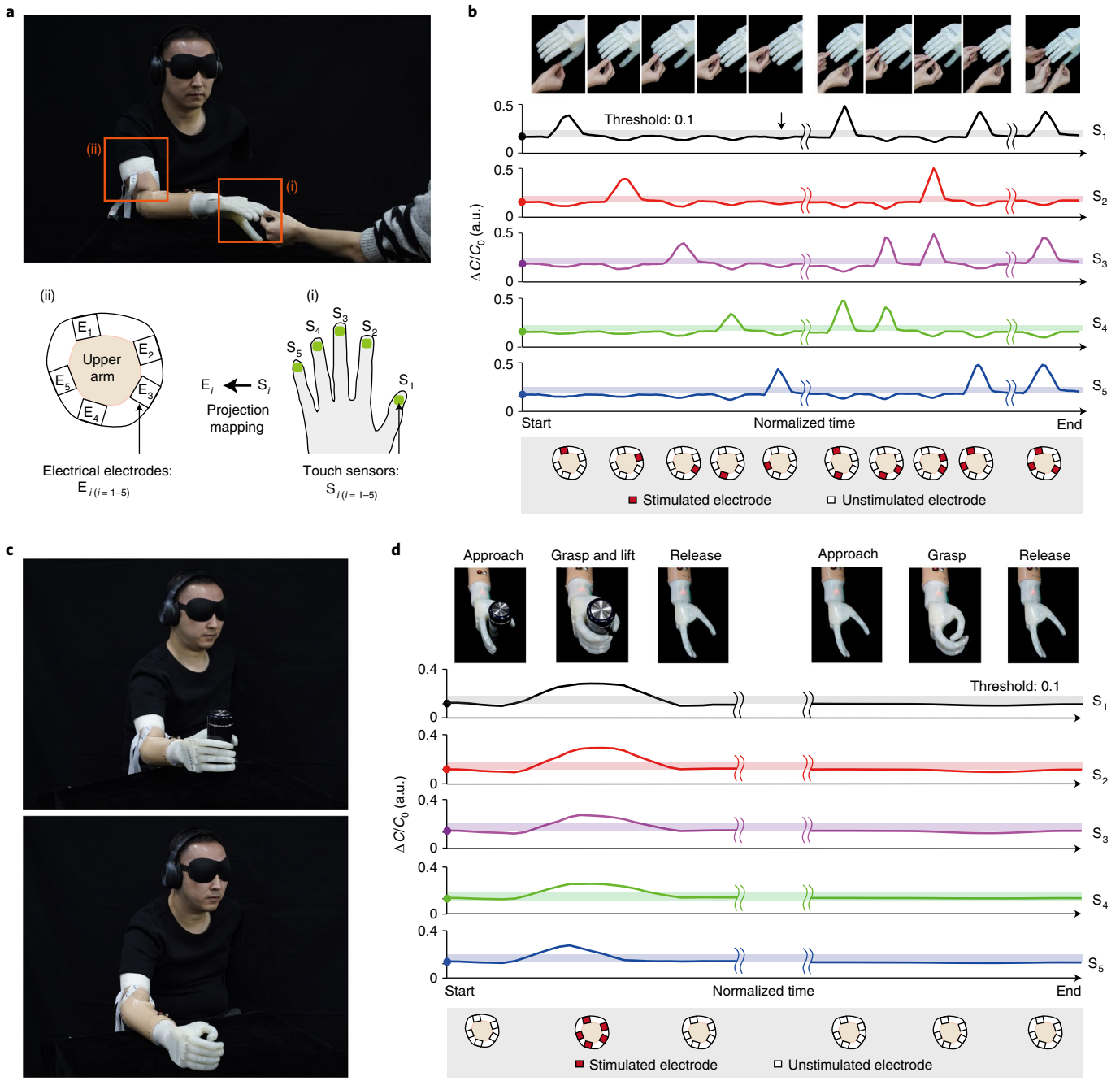

Fig. 4 | An individual with a transradial amputation wearing the soft neuroprosthetic hand, restoring the primitive touch sensation and the closed-loop control in blindfolded and acoustically shielded interaction experiments. a, Touch sensation elicited in the participant (top). Electrical stimulation at five regions (Supplementary Fig. 12) of the residual limb of the individual with an amputation (ii) corresponding to the effective touch pressures above a threshold measured by touch sensors on five fingertips (i) (bottom). **b**, Demonstration of the touch sensation of any individual finger or multiple fingers being compressed (threshold $\Delta C/C_0 = 0.1$, indicated by the shaded area). **c**, Photographs of the individual with an amputation grasping a bottle, sensing the touch pressure and lifting it up (top), or grasping nothing and not lifting up (bottom). **d**, Demonstration of the closed-loop control capability of the soft neuroprosthetic hand enabled by integrating the myoelectric control and tactile feedback. The participant used his own EMG signals to control the soft neuroprosthetic hand to give the power grasp type. If the hand firmly grasped a bottle such that the effective pressures on the five fingertips were above the threshold (threshold, $\Delta C/C_0 = 0.1$, indicated by the shaded area), the participant was informed by the electrical stimulators to lift up the bottle (left, top). By contrast, if the hand did not grasp anything that applied pressure on the fingertips, the individual did not lift up but relaxed the hand after a few seconds (right, top).

We have also experimentally shown that, with sensory feedback, one individual could restore graded tactile sensation and closed-loop control of the soft neuroprosthetic hand. To further improve its performance, advanced EMG-decoding algorithms[48–50] and sensory-feedback approaches[11–18] would need to be implemented. We anticipate that this work will inspire the development of personalized neuroprosthetic hands that are intrinsically soft, lightweight and potentially low cost for individuals with upper-limb amputations.

Methods

Synthesis of the ionic hydrogel. The ionic hydrogel[37–39] is a polyacrylamide (PAAm) hydrogel containing lithium chloride (LiCl). For clarity, below we

reproduce the fabrication method of the ionic hydrogel from ref. [39]. The PAAm-LiCl hydrogel is synthesized using the acrylamide (AAm; J&K) as the monomer, *N*,*N*′-methylenebisacrylamide (MBAA; Molbase) as the crosslinker, LiCl monohydrate ($LiCl{\cdot}H_2O$; Sinopharm Chemical Reagent) as the ionic conductive medium and 2-ketoglutaric acid (Adamas) as the photoinitiator. The monomer solution is prepared by mixing AAm, $LiCl{\cdot}H_2O$ and deionized water at a mass ratio of 9.98%:16.16%:73.86%. MBAA solution is dissolved into deionized water with a mass ratio of 1.2%. The monomer solution, MBAA solution and 2-ketoglutaric acid are then mixed at a mass ratio of 96.67%:1.13%:2.20% to form the hydrogel precursor ink for further fabrication. Note that the LiCl is added into the hydrogel, serving not only as a conductive medium but also as a hygroscopic salt to maintain water in the hydrogel in ambient environments[37–39].

Fabrication and assembly of the soft neuroprosthetic hand. We present a simple and scalable method to fabricate and assemble the soft neuroprosthetic hand (Supplementary Fig. 13). For the soft fingers, we use the Dragon Skin 10 (Smooth-On) silicone rubber for the inner elastomeric tubular structure, the Ecoflex 00-30 (Smooth-On) silicone rubber for the outer elastomeric skin and the polyethylene thread for the fibre reinforcement. We attach the carbon fibre-reinforced plastics lamination with the heat-shrink tubes as the embedded rigid segments of the soft fingers. The palm skeleton is 3D printed with the photosensitive resin (Imagine 8000, SOMOS) and the covered elastomeric skin is made of Ecoflex 00-30 silicone rubber. To tune the colour of the elastomeric skin close to the skin colour of the individual with an amputation, we add Slic Pig pigment PMS 488C (flesh colour, Smooth-On) into the Ecoflex 00-30 silicone rubber (an illustration is provided in Supplementary Fig. 27). The socket is fabricated with the vacuum-forming thermoplastic acrylic resin, and the gold-plated copper blocks are embedded in the socket as the EMG electrodes. We fabricate the capacitive touch sensors by curing the hydrogel precursor (containing acrylamide, crosslinker, photoinitiator and ionic conductive medium) into a very high bond elastomeric matrix. Notably, all of the mechanical components can be constructed with low-cost commercially available materials (Supplementary Table 2). The fabrication and assembly steps of the soft neuroprosthetic hand are described in the Supplementary Information.

Analytical model for the design of the soft finger. The method for efficiently predicting the bending angles of the flexible joints in the soft finger has an important role in mimicking the structure and function of human fingers[24]. We first developed an analytical model to analyse the pneumatic response of a flexible joint. We use a nonlinear elasticity approach to analytically calculate the response of the flexible joint under pneumatic actuation. Specifically, we model the flexible joint as a hollow cuboid of isotropic incompressible neo-Hookean solid with the shear modulus of μ and a stiff inextensible layer beneath the cuboid. We take the thickness, height and width of the hollow cuboid at the undeformed state as t, H and W, respectively (Supplementary Fig. 4a). Owing to the lateral constraint from the stiff fibres surrounding the cuboid, we assume that the cross-sections of the cuboid remain planar after pressurization, which is validated by the finite-element simulation. Furthermore, as the arrangement of fibres are symmetric without twisting, we can express the axial stretch of the cuboid cross-section in a linear form as $\lambda_z(y) = y[\lambda_z(H) - 1]/H + 1$, where $\lambda_z(H) = \lambda_z^H = l/L$ is the axial stretch at the top surface (that is, $y = H$) with l being its elongated length (Supplementary Fig. 4a). The deformation gradient at the side surfaces can be expressed as

$$[\mathbf{F}] = \begin{bmatrix} \lambda_z^{-1}(y) & 0 & 0 \\ 0 & 1 & 0 \\ 0 & 0 & \lambda_z(y) \end{bmatrix} \tag{1}$$

We take the elastomeric cuboid as an incompressible neo-Hookean solid with its strain energy of $W = \mu(\mathbf{F}\mathbf{F}^{\mathrm{T}} - 3)/2$. Therefore, the axial nominal stress in the cuboid is

$$S_{zz}(y) = \mu\left[\frac{y}{H}\left(\lambda_z^H - 1\right) + 1\right] - \mu\left[\frac{y}{H}\left(\lambda_z^H - 1\right) + 1\right]^{-3} \tag{2}$$

Assuming the deformation of the hollow cuboid is pure bending, we can further obtain the geometrical relationship between the bending angle α and the dimensions of the flexible joint (that is, l, L and H)

$$\alpha = \frac{l - L}{H} \tag{3}$$

As the bending actuation is driven by the moment created by the internal pressure imposing on the cap of the flexible joint M_p, the relationship between the pneumatic pressure p and the bending angle α can be found by equating M_p to the moment generated by the internal stress of the elastomeric cuboid M_c. To calculate M_c, we take the stiff inextensible layer as the position of the neutral axis, giving

$$M_c = 2\int_0^H S_{zz}(y) y t \mathrm{d}y + S_{zz}(H) W H t \tag{4}$$

The moment created by the internal pressure is

$$M_p = \int_0^H p W y \mathrm{d}y \tag{5}$$

Solving equations (4) and (5) yields the relationship between the pneumatic pressure and the bending angle as

$$\begin{aligned} &\frac{2t}{3W\left(\lambda_z^H - 1\right)^2}\left[2\left(\lambda_z^H\right)^3 - 3\left(\lambda_z^H\right)^2 + 6\left(\lambda_z^H\right)^{-1} - 3\left(\lambda_z^H\right)^{-2} - 2\right] \\ &+ \frac{2t}{H}\left[\left(\lambda_z^H\right) - \left(\lambda_z^H\right)^{-3}\right] = \frac{p}{\mu} \end{aligned} \tag{6a}$$

$$\lambda_z^H = \alpha\frac{H}{L} + 1 \tag{6b}$$

To verify the analytical model, we further simulate the pneumatic response of the flexible joint, which consists of a cuboid elastomeric chamber, a network of stiff fibres surrounding the elastomeric chamber, and a stiff layer beneath the chamber. We model the elastomeric chamber as a neo-Hookean solid with solid elements (C3D10H), the strain energy density of which is

$$W = \frac{\mu}{2}\left(\mathbf{F}\mathbf{F}^{\mathrm{T}} - 3\right) + \frac{\kappa}{2}(J - 1)^2 \tag{7}$$

where μ is the shear modulus, κ is the bulk modulus, $J = \det(\mathbf{F})$. We set $\mu = 80$ kPa and $\kappa/\mu = 1{,}000$ to impose the nearly incompressibility of the material. The stiff layer is modelled as a skin of shell elements with a Young's modulus of 210 GPa. The fibre is modelled as a beam element (B32H) with a Young's modulus of 1 GPa. The thickness t, width W and height H of the cuboid are set as 1 mm, 8 mm and 8 mm, respectively. The fibre direction is set perpendicular to the axial direction of the finger to constrain the lateral expansion of the flexible joints during inflation[17]. Static simulations are performed by applying pressure on all internal faces of the elastomer chamber with zero displacements at the base portion of the finger as the boundary conditions. We first compare the axial stretch at the top surface of the flexible joint in experiments and simulations, verifying the main deformation mode of the flexible joints is the bending motion (Supplementary Fig. 4b). We further compare the increase in the bending angle α as a function of the applied inflation pressure p for the flexible joints with various lengths in the finite-element simulation and the analytical model, showing good agreement (Supplementary Fig. 4c). Despite the nonlinear large deformation of the elastomeric cuboid, we also show that the bending angle of the joint is almost linearly proportional to its initial length L under a constant inflation pressure p (Supplementary Fig. 4d).

We further study the pneumatic response of a soft finger consisting of an inner hollow cuboid elastomeric tubular structure surrounded by a network of fibres, rigid segments and a stiff layer beneath the elastomeric tube (Supplementary Fig. 5a). Mimicking the dimensions of the distal phalanx, middle phalanx and proximal phalanx in human fingers[17,18], we set the total length of the finger as 85 mm and the length ratio of the top, middle and bottom parts as 2:3:5 in the model (Supplementary Fig. 5a). We show that the ratio of the bending angles of the three joints are nearly constant due to the same pneumatic pressure applied to the three joints (Supplementary Fig. 5b). Moreover, the ratio of the bending angles of the three joints are independent of the total length of all flexible joints $L_D + L_P + L_M$ provided that the ratio of the lengths of the three joints is fixed (for example, $L_D{:}L_P{:}L_M = 2{:}4{:}1$; Supplementary Fig. 5c).

In existing prosthetic hands[1,2], the bending motion of a finger typically follows two characteristics: (1) the bending angle of α_D is approximately half of that of α_M; and (2) the bending angle of α_P is approximately the same as α_M. On the basis of our analysis, we show that the central idea to mimic the motion trajectory of human fingers is to design the length ratio of the three flexible joints. Specifically, the length of the distal interphalangeal joint L_D needs to be half of the length of the metacarpophalangeal joint L_M, while the length of the proximal interphalangeal joint L_P is preferably the same as the length of the metacarpophalangeal joint L_M. Although we analyse the soft fingers with three flexible joints, the conclusion also applies to the thumb with two flexible joints, which will also be verified in the simulation with the finite-element model.

Finite-element model for the design of the soft finger. To further verify the experimental results of the hand with five soft fingers, we developed a finite-element model of the soft fingers in ABAQUS to quantitatively predict the bending angles of the flexible joints and the motion trajectories of the fingers after inflation. All material parameters are experimentally measured from mechanical characterizations[51]. The elastomeric tube is modelled as a neo-Hookean solid (equation (7)) with a shear modulus $\mu = 85$ kPa and a ratio of bulk modulus to shear modulus $\kappa/\mu = 1{,}000$ to impose the near incompressibility of the material. The silicone skins on the outer surface are modelled as a linear elastic material with the elastic modulus 0.125 MPa and Poisson's ratio 0.45. The PE fibres are modelled as a linear elastic material with the Young's modulus 2.9 GPa and Poisson's ratio 0.41. The heat-shrinkable tube is modelled as a linear elastic material with the

Young's modulus 55 MPa and Poisson's ratio 0.4. The carbon-fibre-reinforced plastic is modelled as a linear elastic material with the Young's modulus 210 GPa and Poisson's ratio 0.3. The fibreglass grid is modelled as a linear elastic material with the Young's modulus 73 GPa and Poisson's ratio 0.22.

To reduce the computational cost, we use the skin module to model the heat-shrinkable tube, the carbon fibre-reinforced plastics and the fibreglass grid. The Ecoflex 00–30 layers are modelled as skins with uniform thickness as the outer surfaces of the fibre-reinforced inner elastomeric tube. An extra skin of a stiffer rubber material is added on the surfaces of the thumb–palm connection to model the constraint effect of the silicone layer. The elastomer of the inner tube is modelled as solid elements C3D4H. The fibres are modelled as beam elements B31. Tie constraints are set between the fibres and the elastomeric chambers of the finger actuators, the thumb actuator and the thumb–palm connection actuator. The proximal ends of the thumb–palm connection are fixed to the rigid palm skeleton. The gravity load and a pressure load are applied to the inner surface of the tube of the soft fingers. The finite-element model is in quantitative agreement with the experimental results (Supplementary Fig. 6, Supplementary Table 4 and Supplementary Video 1).

Participant recruitment. All experiments were conducted in accordance with the declaration of Helsinki and approved by the Ethics Committee of Human and Animal Experiments of Shanghai Jiao Tong University. The individuals with transradial amputations who participated in this study were recommended by Shanghai Liankang Prosthetics and Orthotics Manufacturing. The participants did not have any previous neuromuscular disorders, and were informed about the experimental procedure and signed the informed consent forms before participation. The authors affirm that human research participants provided written informed consent for the publication of the images in Figs. 1, 3 and 4, Supplementary Figs. 1, 7, 12, 17, 20, 22, 23 and 25–27, and Supplementary Videos 3–14.

The training process for EMG decoding. During the training process, the individual performing the predefined grasp types (Fig. 2h) is notified by the vibration from a motor placed on the socket. Each grasp type is maintained for 5 s and a rest period is required between two grasp types to prevent possible fatigue of the individual. In the experiments, short-duration vibrations are provided at the beginning and end of each grasp type to notify the individual to transit between different hand grasps, and a long-duration vibration is provided at the end of the training session. Each channel (recorded by each EMG sensor) of the EMG signals from the individual performing a predefined grasp type is segmented into data fragments with 200 ms windows. Thereafter, a time-domain feature set from the data fragments of each channel for the predefined grasp type is extracted, including the mean absolute value, waveform length, zero-crossings and slope sign changes. The features from different channels for the same predefined grasp type are cascaded to give a feature vector. Subsequently, the feature vectors obtained from the training data are fed into the linear discriminant analysis (LDA)[40] classifier (Supplementary Information) to specify the parameters for the predefined grasp types. The whole training session lasts about 15 min (a demonstration of the training process is shown in Supplementary Fig. 20 and Supplementary Video 4).

Although the LDA-based surface EMG decoding algorithms can accurately classify the five classes in laboratory settings (Supplementary Fig. 19), the performance will be reduced for individuals with amputations in realistic activities[52]. Therefore, in many demonstrations of the functions of the soft neuroprosthetic hand, we chose a single grasp classifier on the basis of testing items of the standardized tests. We have indicated in the in the captions for the Supplementary Videos whether either five-class classifier or a single grasp classifier has been chosen.

The training process for tactile feedback. In the training process for tactile feedback, the stimulation current is set as bi-phasic, rectangular current pulses. On the basis of our previous results[53], we set the current amplitudes, pulse widths and frequencies for all five channels as 4 mA, 200 μs and 20 Hz, respectively. During the training process, we compress each soft finger three times in a random order to check whether the individual can discriminate the compressed finger on the basis of the electrical stimulation. The training process lasts about 5 min.

Data analysis and statistics. All data were analysed using the available built-in functions of MATLAB (R2016b, MathWorks) and SPSS (version 22, IBM). All data are reported as mean values with s.d. when indicated. In the statistical analyses of standardized tests, the factors (independent variables) are the neuroprosthetic hand type (the soft neuroprosthetic hand and the rigid neuroprosthetic hand) and task type (items J2–J7 or S1–S9). The dependent variable is the task time. All data were demonstrated to be normally distributed, determined using the Kolgomorov–Smirnov test ($P > 0.05$) before analysis for statistical significance. Two-way ANOVA was used to statistically analyse the significant influences of the two factors (neuroprosthetic hand types and task types) on the task time in the two sessions (items J2–J7 or S1–S9). According to two-way ANOVA, there is interaction between the two factors. Bonferroni correction was used to correct for multiple comparisons. Two-tailed, paired-sample *t*-tests were used to compare the difference in blocks per minute (in the box and blocks test) or words per minute (item J1) with different neuroprosthetic hand types.

Reporting Summary. Further information on research design is available in the Nature Research Reporting Summary linked to this article.

Data availability

The main data supporting the results in this study are available within the paper and its Supplementary Information. Source data for Fig. 3a and Supplementary Figs. 23 and 26 are available as Supplementary Information. All data needed to evaluate the conclusions are presented in the paper and the Supplementary Information.

Received: 22 February 2020; Accepted: 21 June 2021;
Published online: 16 August 2021

References

1. Cordella, F. et al. Literature review on needs of upper limb prosthesis users. *Front. Neurosci.* **10**, 209 (2016).
2. Belter, J. T., Segil, J. L., Dollar, A. M. & Weir, R. F. Mechanical design and performance specifications of anthropomorphic prosthetic hands: a review. *J. Rehabil. Res. Dev.* **50**, 599–618 (2013).
3. Lewis, S., Russold, M. F., Diet, H. & Kaniusas, E. Satisfaction of prosthesis users with electrical hand prostheses and their sugggested improvements. *Biomed. Tech.* https://doi.org/10.1515/bmt-2013-4385 (2013).
4. Biddiss, W. A. & Chau, T. T. Upper limb prosthesis use and abandonment: a survey of the last 25 years. *Prosthet. Orthot. Int.* **31**, 236–257 (2007).
5. Farina, D. & Aszmann, O. Bionic limbs: clinical reality and academic promises. *Sci. Transl. Med.* **6**, 257ps12 (2014).
6. Carey, S. L., Lura, D. J. & Highsmith, M. J. Differences in myoelectric and body-powered upper-limb prostheses: systematic literature review. *J. Rehabil. Res. Dev.* **52**, 247–262 (2015).
7. Xu, K., Guo, W., Hua, L., Sheng, X. & Zhu, X. A prosthetic arm based on EMG pattern recognition. In *Proc. IEEE International Conference on Robotics and Biomimetics (ROBIO)* 1179–1184 (IEEE, 2016).
8. Catalano, M. G. et al. Adaptive synergies for the design and control of the Pisa/IIT SoftHand. *Int. J. Robot. Res.* **33**, 768–782 (2014).
9. Godfrey, S. B. et al. The SoftHand Pro: functional evaluation of a novel, flexible, and robust myoelectric prosthesis. *PLoS ONE* **13**, e0205653 (2018).
10. Kanzler, C. M. et al. An objective functional evaluation of myoelectrically-controlled hand prostheses: a pilot study using the virtual peg insertion test. In *Proc. 2019 IEEE 16th International Conference on Rehabilitation Robotics (ICORR)* 392–397 (2019).
11. Tan, D. W. et al. A neural interface provides long-term stable natural touch perception. *Sci. Transl. Med.* **6**, 257ra138 (2014).
12. Raspopovic, S. et al. Restoring natural sensory feedback in real-time bidirectional hand prostheses. *Sci. Transl. Med.* **6**, 222ra19 (2014).
13. Clemente, F. et al. Non-Invasive, temporally discrete feedback of object contact and release improves grasp control of closed-loop myoelectric transradial prostheses. *IEEE Trans. Neural Syst. Rehabil. Eng.* **24**, 1314–1322 (2016).
14. D'Anna, E. et al. A somatotopic bidirectional hand prosthesis with transcutaneous electrical nerve stimulation based sensory feedback. *Sci. Rep.* **7**, 10930 (2017).
15. Valle, G. et al. Biomimetic intraneural sensory feedback enhances sensation naturalness, tactile sensitivity, and manual dexterity in a bidirectional prosthesis. *Neuron* **100**, 37–45 (2018).
16. Osborn, L. E. et al. Prosthesis with neuromorphic multilayered e-dermis perceives touch and pain. *Sci. Robot.* **3**, eaat3818 (2018).
17. Zollo, L. et al. Restoring tactile sensations via neural interfaces for real-time force-and-slippage closed-loop control of bionic hands. *Sci. Robot.* **4**, eaau9924 (2019).
18. D'Anna, E. et al. A closed-loop hand prosthesis with simultaneous intraneural tactile and position feedback. *Sci. Robot.* **4**, eaau8892 (2019).
19. Rus, D. & Tolley, M. T. Design, fabrication and control of soft robots. *Nature* **521**, 467–475 (2015).
20. Rich, S. I., Wood, R. J. & Majidi, C. Untethered soft robotics. *Nat. Electron.* **1**, 102–112 (2018).
21. Polygerinos, P. et al. Soft Robotics: review of fluid-driven intrinsically soft devices; manufacturing, sensing, control, and applications in human-robot interaction. *Adv. Eng. Mater.* **19**, 1700016 (2017).
22. Hu, W., Lum, G. Z., Mastrangeli, M. & Sitti, M. Small-scale soft-bodied robot with multimodal locomotion. *Nature* **554**, 81–85 (2018).
23. Acome, E. et al. Hydraulically amplified self-healing electrostatic actuators with muscle-like performance. *Science* **359**, 61–65 (2018).
24. Connolly, F., Walsh, C. J. & Bertoldi, K. Automatic design of fiber-reinforced soft actuators for trajectory matching. *Proc. Natl Acad. Sci. USA* **114**, 51–56 (2017).

25. Cacucciolo, V. et al. Stretchable pumps for soft machines. *Nature* **572**, 516–519 (2019).
26. Farrow, N. & Correll, N. A soft pneumatic actuator that can sense grasp and touch. In *Proc. IEEE International Conference on Intelligent Robots and Systems (IROS)* 2317–2323 (IEEE, 2015).
27. Ferris, D. P. & Lewis, C. L. Robotic lower limb exoskeletons using proportional myoelectric control. In *Proc. IEEE Engineering in Medicine and Biology Society Annual Conference* 2119–2124 (2009).
28. Polygerinos, P. et al. EMG controlled soft robotic glove for assistance during activities of daily living. In *Proc. IEEE International Conference on Rehabilitation Robotics (ICORR)* 55–60 (IEEE, 2015).
29. Ge, L. et al. Design, modeling, and evaluation of fabric-based pneumatic actuators for soft wearable assistive gloves. *Soft Robot.* **7**, 583–596 (2020).
30. Deimel, R. & Brock, O. A novel type of compliant and underactuated robotic hand for dexterous grasping. *Int. J. Robot. Res.* **35**, 161–185 (2016).
31. Scharff et al. In *Soft Robotics: Rends, Applications and Challenges* (eds Laschi, C. et al.) 23–29 (Springer, 2017).
32. Zhao, H., O'Brien, K., Li, S. & Shepherd, R. F. Optoelectronically innervated soft prosthetic hand via stretchable optical waveguides. *Sci. Robot.* **1**, 7529 (2016).
33. Zhou, J. et al. BCL-13: a 13-DOF soft robotic hand for dexterous grasping and in-hand manipulation. *IEEE Robot. Autom. Lett.* **3**, 3379–3386 (2018).
34. Zhou, J. et al. A Soft-robotic approach to anthropomorphic robotic hand dexterity. *IEEE Access* **7**, 101483–101495 (2019).
35. Emerson, E. T., Krizek, T. J. & Greenwald, D. P. Anatomy, physiology, and functional restoration of the thumb. *Ann. Plast. Surg.* **36**, 180–191 (1996).
36. Gustus, A., Stillfried, G., Visser, J., Jörntell, H. & Smagt, P. Human hand modelling: kinematics, dynamics, applications. *Biol. Cybern.* **106**, 741–755 (2012).
37. Keplinger, C. et al. Stretchable, transparent, ionic conductors. *Science* **341**, 984–987 (2013).
38. Yang, C. & Suo, Z. Hydrogel ionotronics. *Nat. Rev. Mater.* **3**, 125–142 (2018).
39. Gu, G. et al. Integrated soft ionotronic skin with stretchable and transparent hydrogel-elastomer ionic sensors for hand-motion monitoring. *Soft Robot.* **6**, 368–376 (2019).
40. Englehart, K. & Hudgins, B. A robust, real-time control scheme for multifunction myoelectric control. *IEEE Trans. Biomed. Eng.* **50**, 848–854 (2003).
41. Feix, T., Romero, J., Schmiedmayer, H., Dollar, A. M. & Kragic, D. The GRASP taxonomy of human grasp types. *IEEE Trans. Hum. Mach. Syst.* **46**, 66–77 (2016).
42. Bullock, I. M. et al. Grasp frequency and usage in daily household and machine shop tasks. *IEEE Trans. Haptics* **6**, 296–308 (2013).
43. Kyberd, P. J., Evans, M. & Winkel, S. An intelligent anthropomorphic hand, with automatic Grasp. *Robotica* **16**, 531–536 (1998).
44. Hammock, M. L., Chortos, A., Tee, B., Tok, J. & Bao, Z. 25th anniversary article: the evolution of electronic skin (e-skin): a brief history, design considerations, and recent progress. *Adv. Mater.* **25**, 5997–6038 (2013).
45. Resnik, L. & Borgia, M. Reliability and validity of outcome measures for upper limb amputation. *JPO J. Prosthet. Orthot.* **24**, 192–201 (2012).
46. Phillips, S. L., Harris, M. S., Koss, L. & Latlief, G. Experiences and outcomes with powered partial hand prostheses: a case series of subjects with multiple limb amputations. *JPO J. Prosthet. Orthot.* **24**, 93–97 (2012).
47. Smit, G., Plettenburg, D. & Helm, F. The lightweight delft cylinder hand, the first multi-articulating hand that meets the basic user requirements. *IEEE Trans. Neural Syst. Rehabil. Eng.* **23**, 431–440 (2015).
48. Fougner, A. et al. Control of upper limb prostheses: terminology and proportional myoelectric control—a review. *IEEE Trans. Neural Syst. Rehabil. Eng.* **20**, 663–677 (2012).
49. Hahne, J. M. et al. Simultaneous control of multiple functions of bionic hand prostheses: performance and robustness in end users. *Sci. Robot.* **3**, eaat3630 (2018).
50. Zhuang, K. Z. et al. Shared human-robot proportional control of a dexterous myoelectric prosthesis. *Nat. Mach. Intell.* **1**, 400–411 (2019).
51. Jones, D. R. H & Ashby, M. F. *Engineering Materials 1: An Introduction to Properties, Applications and Design* 4th edn (Butterworth-Heinemann, 2011).
52. Farina, D. et al. The extraction of neural information from the surface EMG for the control of upper-limb prostheses: emerging avenues and challenges. *IEEE Trans. Neural Syst. Rehabil. Eng.* **22**, 797–809 (2014).
53. Chai, G. et al. Characterization of evoked tactile sensation in forearm amputees with transcutaneous electrical nerve stimulation. *J. Neural Eng.* **12**, 066002 (2015).

Acknowledgements

We thank the participants for agreeing to participate in this research; M. Feng, Z. Shen, X. Huang and N. Ding for their participation in building the experimental set-ups; and Q. He for the discussions of the model and simulation. This study was supported in part by the National Natural Science Foundation of China (grant nos 91948302, 52025057 and 51620105002), the Science and Technology Commission of Shanghai Municipality (grant no. 20550712100), Shanghai Jiao Tong University Scientific and Technological Innovation Funds, and Massachusetts Institute of Technology.

Author contributions

G.G., N.Z., X. Zhu and X. Zhao conceived the idea and designed the study. G.G., N.Z., H.X., H.Y., Q.S. and X. Zhu performed experiments and analysed the experimental data. Y.Y., G.C., X.S. and X. Zhu developed the EMG sensors and electrical stimulation platform. G.G., S.L., L.G. and X. Zhao developed the theoretical model and performed the FEM simulation for verification. G.G., X. Zhu and X. Zhao directed the project. G.G., N.Z., H.X., X. Zhu and X. Zhao prepared the manuscript and all of the authors provided feedback and agree with the final version of the manuscript.

Competing interests

G.G., N.Z., H.X., S.L., X. Zhu and X. Zhao are listed as co-inventors on a patent application (US application no. 63/039,929) that covers the design and fabrication of the soft neuroprosthetic hand.

Additional information

Supplementary information The online version contains supplementary material available at https://doi.org/10.1038/s41551-021-00767-0.

Correspondence and requests for materials should be addressed to G.G., X. Zhu or X. Zhao.

Peer review information *Nature Biomedical Engineering* thanks the anonymous reviewers for their contribution to the peer review of this work.

Reprints and permissions information is available at www.nature.com/reprints.

Publisher's note Springer Nature remains neutral with regard to jurisdictional claims in published maps and institutional affiliations.

nature research

Corresponding author(s): Guoying Gu, Xiangyang Zhu, Xuanhe Zhao

Last updated by author(s): Jun 10, 2021

Reporting Summary

Nature Research wishes to improve the reproducibility of the work that we publish. This form provides structure for consistency and transparency in reporting. For further information on Nature Research policies, see our Editorial Policies and the Editorial Policy Checklist.

Statistics

For all statistical analyses, confirm that the following items are present in the figure legend, table legend, main text, or Methods section.

n/a	Confirmed	
☐	☒	The exact sample size (*n*) for each experimental group/condition, given as a discrete number and unit of measurement
☐	☒	A statement on whether measurements were taken from distinct samples or whether the same sample was measured repeatedly
☐	☒	The statistical test(s) used AND whether they are one- or two-sided *Only common tests should be described solely by name; describe more complex techniques in the Methods section.*
☐	☒	A description of all covariates tested
☐	☒	A description of any assumptions or corrections, such as tests of normality and adjustment for multiple comparisons
☐	☒	A full description of the statistical parameters including central tendency (e.g. means) or other basic estimates (e.g. regression coefficient) AND variation (e.g. standard deviation) or associated estimates of uncertainty (e.g. confidence intervals)
☐	☒	For null hypothesis testing, the test statistic (e.g. *F*, *t*, *r*) with confidence intervals, effect sizes, degrees of freedom and *P* value noted *Give P values as exact values whenever suitable.*
☒	☐	For Bayesian analysis, information on the choice of priors and Markov chain Monte Carlo settings
☒	☐	For hierarchical and complex designs, identification of the appropriate level for tests and full reporting of outcomes
☒	☐	Estimates of effect sizes (e.g. Cohen's *d*, Pearson's *r*), indicating how they were calculated

Our web collection on statistics for biologists contains articles on many of the points above.

Software and code

Policy information about availability of computer code

Data collection	No software was used for data collection.
Data analysis	All data were analysed by using the available built-in functions of MATLAB (R2016b, The Mathworks Inc., USA) and SPSS (version 22, IBM Inc., USA).

For manuscripts utilizing custom algorithms or software that are central to the research but not yet described in published literature, software must be made available to editors and reviewers. We strongly encourage code deposition in a community repository (e.g. GitHub). See the Nature Research guidelines for submitting code & software for further information.

Data

Policy information about availability of data

All manuscripts must include a data availability statement. This statement should provide the following information, where applicable:

- Accession codes, unique identifiers, or web links for publicly available datasets
- A list of figures that have associated raw data
- A description of any restrictions on data availability

The main data supporting the results in this study are available within the paper and its Supplementary Information. Source data for Fig. 3a and Supplementary Figs. 23 and 26 are available as Supplementary Information.

Field-specific reporting

Please select the one below that is the best fit for your research. If you are not sure, read the appropriate sections before making your selection.

☒ Life sciences ☐ Behavioural & social sciences ☐ Ecological, evolutionary & environmental sciences

For a reference copy of the document with all sections, see nature.com/documents/nr-reporting-summary-flat.pdf

Life sciences study design

All studies must disclose on these points even when the disclosure is negative.

Sample size	No sample-size calculation was performed, because the experiments and demonstrations were carried out for proof-of-concept.
Data exclusions	No data were excluded from the analyses.
Replication	At least 3 trials for each test were taken and used in the data analysis.
Randomization	Subjects were equipped with a single soft neuroprosthetic hand. Consequently, no randomization was performed.
Blinding	The personnel completing the data analyses were blinded to the experimental groups.

Reporting for specific materials, systems and methods

We require information from authors about some types of materials, experimental systems and methods used in many studies. Here, indicate whether each material, system or method listed is relevant to your study. If you are not sure if a list item applies to your research, read the appropriate section before selecting a response.

Materials & experimental systems

n/a	Involved in the study
☒	☐ Antibodies
☒	☐ Eukaryotic cell lines
☒	☐ Palaeontology and archaeology
☒	☐ Animals and other organisms
☐	☒ Human research participants
☒	☐ Clinical data
☒	☐ Dual use research of concern

Methods

n/a	Involved in the study
☒	☐ ChIP-seq
☒	☐ Flow cytometry
☒	☐ MRI-based neuroimaging

Human research participants

Policy information about studies involving human research participants

Population characteristics	The participants in the standard tests and closed-loop control experiments are transradial amputees.
Recruitment	This was a prospective, non-randomized study to validate the devices. The transradial amputees who participated in this study were recommended by Shanghai Liankang Prosthetics and Orthotics Manufacturing Co. Ltd, Shanghai, China. The amputees did not have any prior neuromuscular disorders, were informed about the experimental procedure, and signed the informed consent forms prior to their participation.
Ethics oversight	All experiments were conducted in accordance with the declaration of Helsinki and approved by the Ethics Committee of Human and Animal Experiments of Shanghai Jiao Tong University. Human research participants provided written informed consent for the publication of the images.

Note that full information on the approval of the study protocol must also be provided in the manuscript.